THE JOURNAL OF PHYSICAL CHEMISTRY Letters

pubs.acs.org/JPCL Letter

Transition Dipole Moments of n = 1, 2, and 3 Perovskite Quantum Wells from the Optical Stark Effect and Many-Body Perturbation Theory

Andrew H. Proppe,◆ Grant W. Walters,◆ Abdullah Y. Alsalloum, Ayan A. Zhumekenov, Edoardo Mosconi, Shana O. Kelley, Filippo De Angelis, Lyudmyla Adamska, Paolo Umari,* Osman M. Bakr,* and Edward H. Sargent*

Cite This: J. Phys. Chem. Lett. 2020, 11, 716−723

Read Online

ACCESS | Metrics & More | Article Recommendations | Supporting Information

ABSTRACT: Metal halide perovskite quantum wells (PQWs) are quantum and dielectrically confined materials exhibiting strongly bound excitons. The exciton transition dipole moment dictates absorption strength and influences interwell coupling in dipole-mediated energy transfer, a process that influences the performance of PQW optoelectronic devices. Here we use transient reflectance spectroscopy with circularly polarized laser pulses to investigate the optical Stark effect in dimensionally pure single crystals of n = 1, 2, and 3 Ruddlesden−Popper PQWs. From these measurements, we extract in-plane transition dipole moments of 11.1 (±0.4), 9.6 (±0.6) and 13.0 (±0.8) D for n = 1, 2 and 3, respectively. We corroborate our experimental results with density functional and many-body perturbation theory calculations, finding that the nature of band edge orbitals and exciton wave function delocalization depends on the PQW "odd−even" symmetry. This accounts for the nonmonotonic relationship between transition dipole moment and PQW dimensionality in the n = 1−3 range.

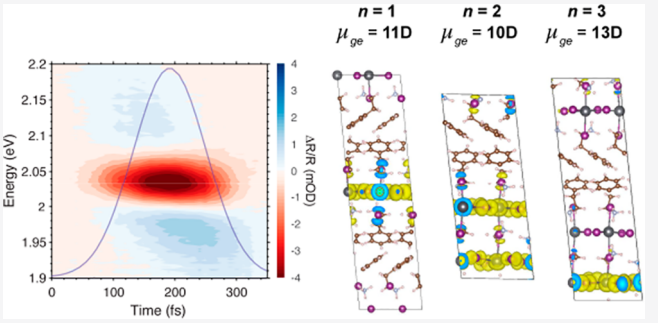

Metal halide perovskites are solution- and vacuum-processed semiconductors that possess remarkable optoelectronic properties and have been used to fabricate efficient photovoltaics,[1−3] light-emitting diodes,[4−8] and lasers.[9] Low-dimensional analogues of these materials can be synthesized by using large alkyl or aryl ammonium ligands to bisect the 3D perovskite lattice along one axis into a finite number of monolayers, n.[10−14] These low-dimensional perovskites, quantum confined along the axis of lattice termination, exhibit the 2D electronic structure of a quantum well[15−17] and strongly bound excitons. Dielectric confinement by organic ligands further increases the exciton binding energy,[17,18] values of which have been reported to be in the range of hundreds of millielectronvolts.[19,20] Both types of confinement contribute to increased optical transition strengths, which scale with exciton binding energy.[21]

Variations in the degree of confinement across the range of perovskite quantum well (PQW) thicknesses cause thin films of mixed-dimensionality multiple PQWs to possess largely fluctuating energy landscapes. The band alignment between PQWs leads to an energy gradient that funnels excitons and carriers to the smallest band gap PQWs, leading to improved photoluminescence quantum yields and high external quantum efficiencies for solution-processed LED devices[4−6,8] and efficient luminescent solar concentrators, where Stokes shift engineering is possible through control of mixed PQW dimensionality.[22]

This energy funneling has been shown by multiple groups to occur on ultrafast time scales (hundreds of femtoseconds to a few picoseconds).[5,7,22−24] Recent multidimensional spectroscopy measurements have suggested that ultrafast exciton transfer occurs between oriented PQWs via a Förster resonant energy transfer (FRET) mechanism.[25] A key determinant of FRET rates (derived from Fermi's golden rule)[26] is the electronic coupling element between donor and acceptor. When donor and acceptor chromophores are separated beyond their van der Waals radii, interchromophore (or interwell) coupling can be described by the Coulombic interaction between the transition charge densities of the donor and acceptor species.[27] This transition charge density between ground (g) and excited (e) states is often approximated as the first term of its multipole expansion (dipole approximation)[28] and is known as the transition dipole moment (μ_{ge}).[26,29,30]

Received: November 12, 2019
Accepted: January 14, 2020
Published: January 14, 2020

https://dx.doi.org/10.1021/acs.jpclett.9b03349
J. Phys. Chem. Lett. 2020, 11, 716−723

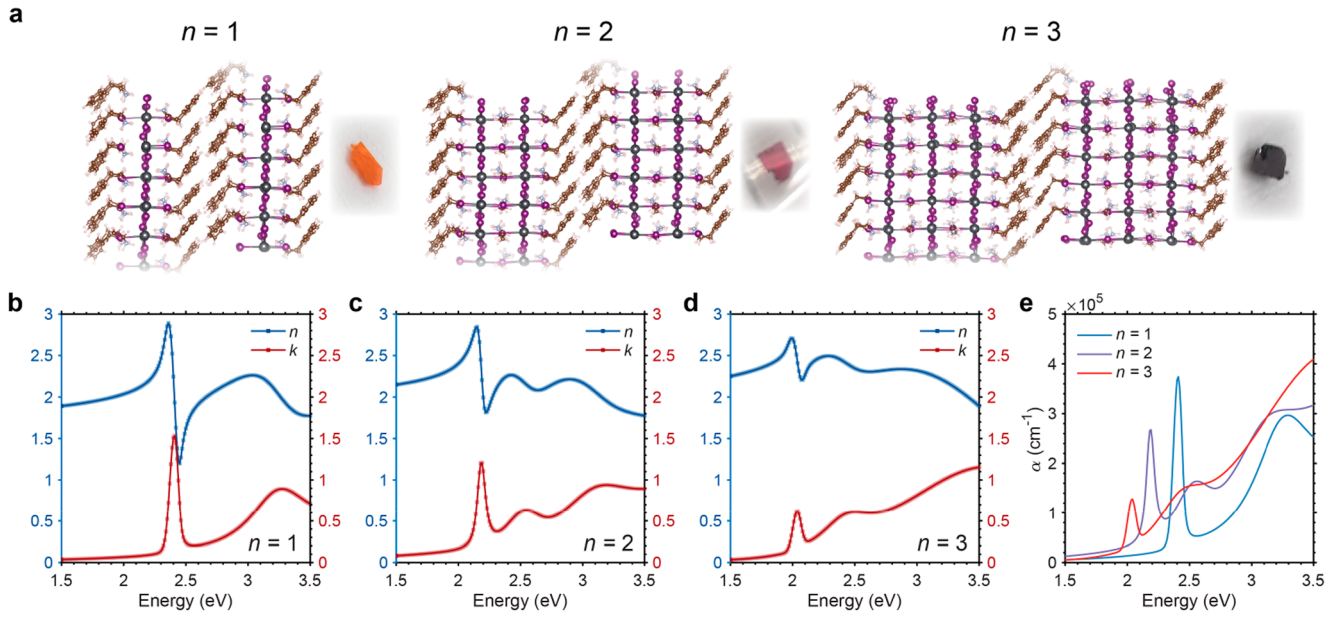

Figure 1. (a) Molecular structure of n = 1, 2, and 3 perovskites depicted with phenylethylammonium bilayers separating two QWs. Photographs of the single crystals mounted on glass substrates are shown beside each respective structure. (b–d) Optical constants and (e) absorption coefficients obtained from ellipsometry measurements for the three single crystals. The lack of other sharp excitonic features besides the main exciton peak for each single crystal verifies their dimensional purity.

Larger transition dipoles favor stronger interwell coupling and therefore faster energy transfer. In addition to magnitude, the electronic coupling is also influenced by the relative orientation of μ between donor and acceptor. In PQWs and other quantum-confined two-dimensional semiconductors, the transition dipole moment should be oriented in the plane of the well.[31−33] Gao et al. confirmed the in-plane orientation for the transition dipole moments of CdSe nanoplatelets and MoS_2 monolayers using back focal plane imaging.[34] Rowland et al. have shown that solids consisting of cofacially aligned CdSe quantum wells, owing to the strong electronic coupling afforded by the in-plane orientation of μ in these 2D materials, exhibited rapid interwell FRET that could outpace Auger recombination.[35] Furthermore, μ is proportional to the oscillator strength, f, of an optical transition,[28] which is fundamental to the electronic structure of the ground and excited states and determines the absorption cross section and Einstein coefficients of a given material.[36] It is therefore of interest to determine the magnitude of the in-plane component of μ_{ge} in PQWs and the relationship between μ_{ge} and PQW dimensionality, because such knowledge could inform how to achieve stronger coupling (and faster energy transfer) between donor and acceptor wells for more efficient exciton funneling, which may be beneficial to mixed-PQW materials used in LEDs,[5,7,8] lasers,[37] and luminescent solar concentrators.[22]

Although μ and f of a material can be related to its absorption coefficient (the relationships between absorption cross sections, μ, f, and Einstein coefficients are thoroughly described by Hilborn in ref 36), μ can be directly quantified from ultrafast transient reflectance measurements revealing the optical Stark effect (OSE). In an OSE experiment, a broadband probe pulse is spatially and temporally overlapped with a nonresonant (sub-band gap) "pump" pulse that, because of the oscillating electric field of the pulse, shifts the energy levels of the ground and excited states—only during the duration of the pulse. Detailed quantum mechanical and semiclassical treatments of this phenomenon can be found in ref 38−40. As this shift occurs only during the duration of the pump pulse, the energy shift can be calculated by comparing pump-on and pump-off transient reflectance spectra during the pump and probe overlap, which results in a derivative-like spectral feature centered around the optical transition. The energy shift, ΔE, is proportional to μ_{ge}:[38]

$$\Delta E = \frac{\mu_{ge}^{2}\varepsilon_{0}^{2}}{\Delta} \tag{1}$$

where ε_0^2 is the time-averaged value of the electric field squared due to the nonresonant pump pulse (which can be calculated from excitation fluence) and Δ is the detuning of the pump pulse relative to the energy of the optical transition.

While OSE experiments providing estimates of μ_{ge} have been reported for dimensionally pure thin films of 2D (n = 1)[41] and 3D perovskites,[42] there are no theoretical studies to offer a physical or mechanistic basis of comparison with these experimental values and no reports of transition dipole moments for PQWs of higher dimensionality. One factor militating against such combined experimental−theoretical studies is the lack of dimensional purity among the quasi-two-dimensional perovskites making up spin-coated thin films.

We reasoned that the growth of single crystals of dimensionally pure PQWs[43−45] could enable the experimental study of OSE and comparison with theory for a series of highly confined PQWs having well-defined well thicknesses. We use ultrafast transient reflectance spectroscopy and ellipsometry on dimensionally pure single crystals of n = 1, 2, and 3 lead iodide PQWs and, from the observed OSE, extract in-plane values of μ_{ge} for these materials for the first time. We experimentally obtain μ_{ge} of 11.1 (±0.4), 9.6 (±0.6), and 13.0 (±0.8) D for n = 1, 2, and 3, respectively. The nonmonotonic trend seen in the experimental values is shown theoretically using density functional theory (DFT) and many-body perturbation theory

https://dx.doi.org/10.1021/acs.jpclett.9b03349
J. Phys. Chem. Lett. 2020, 11, 716−723

(MBPT). We account for the "odd−even" relationship between μ_{ge} and dimensionality through the stronger localization of the highest occupied molecular orbital (HOMO) in n = 1 and 3 and greater delocalization of the HOMO in n = 2, arising because of greater symmetry within these bilayer materials. These dipole moments are significantly higher than those found in analogous inorganic QW systems (e.g., 6.4 D for GaAlAs,[46] 6.2 D for InGaAs[47]) and are close in magnitude to values measured in single-walled carbon nanotubes (11.8 D).[48]

The crystal structures of the n = 1, 2, and 3 PQWs are shown in Figure 1a. Details of the single crystal growth can be found in the Supporting Information. In brief, the crystals were grown using a slow-cooling method with a heated and saturated precursor solution. As reported previously,[49] this method produces crystals that have physical dimensions that span several millimeters and are dimensionally pure. X-ray diffraction (XRD) patterns display no observable peaks corresponding to PQWs with different widths than the expected n value (Figure S1).[50] The phase purity and large dimensions were necessary to ensure accurate quantification of these materials' optical properties and Stark shifts.

We used spectroscopic ellipsometry to measure the real and imaginary parts of the dielectric function, results which were used for optical modeling imperative to the determination of the Stark shifts from the transient reflectance experiments. Scattering was minimized in ellipsometry measurements by exfoliating the crystals several times to expose clean surfaces. Strong signal intensities were achieved in all the measurements, indicating that the crystal surfaces were smooth. In addition, thick crystals were chosen for the measurements such that they could be considered as substrates in the modeling. The optical constants of the complex refractive index, $\tilde{n} = n + ik$, for each material are provided in Figure 1b−d. The spectra for the crystals exhibit strong anomalous dispersion and absorption at the excitonic resonances, exemplifying the dimensional purity of the samples. The absorption coefficients (Figure 1e and Table 1) scale with well width, a confluence of changes in packing density of the wells as well as possible changes in μ_{ge} and the density of states (DOS). Although the absorption coefficient directly depends on the transition dipole moment (and so the oscillator strength), it also depends on the joint DOS and the Fermi functions. The differences in the densities of the quantum wells within the materials is a significant contributor. As n decreases, the spacing between the number of quantum wells per length of material increases. We include a more detailed discussion regarding the relationship between the transition dipole moment and the absorption coefficient in the Supporting Information.

Table 1. Optical Properties Extracted from Ellipsometry Measurements and Experimental Parameters for OSE Experiments

crystal	exciton peak (eV)	α_{peak} (cm^{-1})	detuning (eV)	n (1.65 eV)
n = 1	2.41	374 000	0.76	1.92
n = 2	2.19	278 000	0.54	2.19
n = 3	2.04	128 000	0.39	2.30

In recently reported OSE experiments on 2D materials such as perovskite QWs or transition metal dichalcogenides like monolayer WS_2,[38] circularly polarized pump and probe pulses have been used in order to characterize the extent to which this effect breaks valley degeneracy. The transient signals arising from OSE are maximized when pump and probe pulses are cocircularly polarized and are absent when cross-circularly polarized.[38,41,42]

We take advantage of this selectivity herein in order to remove signals unrelated to OSE that may influence the magnitude of the measured ΔR signals. All experiments are therefore performed with co- and cross-circularly polarized pulses, and then the cross-polarized data is subtracted from the copolarized data for analysis. Further discussions of experimental considerations used to obtain accurate estimates of μ_{ge} can be found in the Supporting Information. Figure S3 shows a representative 2D transient reflectance map of the signals caused by the OSE in a single crystal of n = 3 using detuned pump pulses with a central wavelength of 750 nm (1.65 eV). The positive and negative derivative-like spectral features are centered about the excitonic transition. Deviation from the typical derivative-like feature was also observed, a result of the sensitivity of reflection-mode measurements to refractive index changes associated with the changes to the absorption coefficients.

Transient reflectance spectral traces obtained using pump pulses with energies of 1.65 eV and intensities ranging from 1.21−4.45 $GW{\cdot}cm^{-2}$ for the n = 1, 2, and 3 crystals are shown in Figure 2a−c. In order to obtain ΔE, we fit these spectral traces with simulated transient reflectance spectra. Utilizing the optical constants determined with ellipsometry, the simulated spectra were calculated with an optical model that produced reflectance spectra for the crystals in pump-on and pump-off cases. For the pump-on case, changes to the absorption coefficient following

$$\Delta\alpha = -\frac{1}{2}\frac{d\alpha}{dE}\Delta E \tag{2}$$

were added and corresponding changes to the refractive indices were calculated and added as well. The simulated spectra were fit to the experimental data by varying ΔE to minimize the differences in absolute area of the spectra. The energy shifts, plotted as a function of pump intensity (Figure 2d), were then used with eq 1 to determine the values of μ_{ge}. The shifts in energy follow the expected linear trend, with their slopes increasing with n value. The calculated values of μ_{ge} were found to be 11.1 (±0.4), 9.6 (±0.6), and 13.0 (±0.8) for the n = 1, 2, and 3 crystals, respectively. We note some apparent discrepancies between peak positions and amplitudes in the raw versus fitted transient reflectance data. These arise because we fit ΔE to minimize the differences in the spectral weight transfer (SWT), the area of the curve, between the empirical and simulated curves. In addition to eq 2, the relation between changes in absorption and Stark shift can also be written in integral form, following Sie et al.:[51]

$$\int_{E_0}^{\infty} \Delta\alpha\, dE = \alpha\Delta E = \mathrm{SWT} \tag{3}$$

which clearly shows the importance of the area of the curve, rather than the positions or amplitudes of spectral features, in elucidating the Stark shifts. Uncertainties are calculated from the mean squared error of ΔE. Details about modeling, fitting, and uncertainties in ΔE and μ_{ge} are included in the Supporting Information (methods and supplemental discussion).

To gain insight into the optical properties of the PQW materials, we carried out DFT and MBPT simulations on the n = 1−3 series using the Quantum Espresso program package.[52]

https://dx.doi.org/10.1021/acs.jpclett.9b03349
J. Phys. Chem. Lett. 2020, 11, 716−723

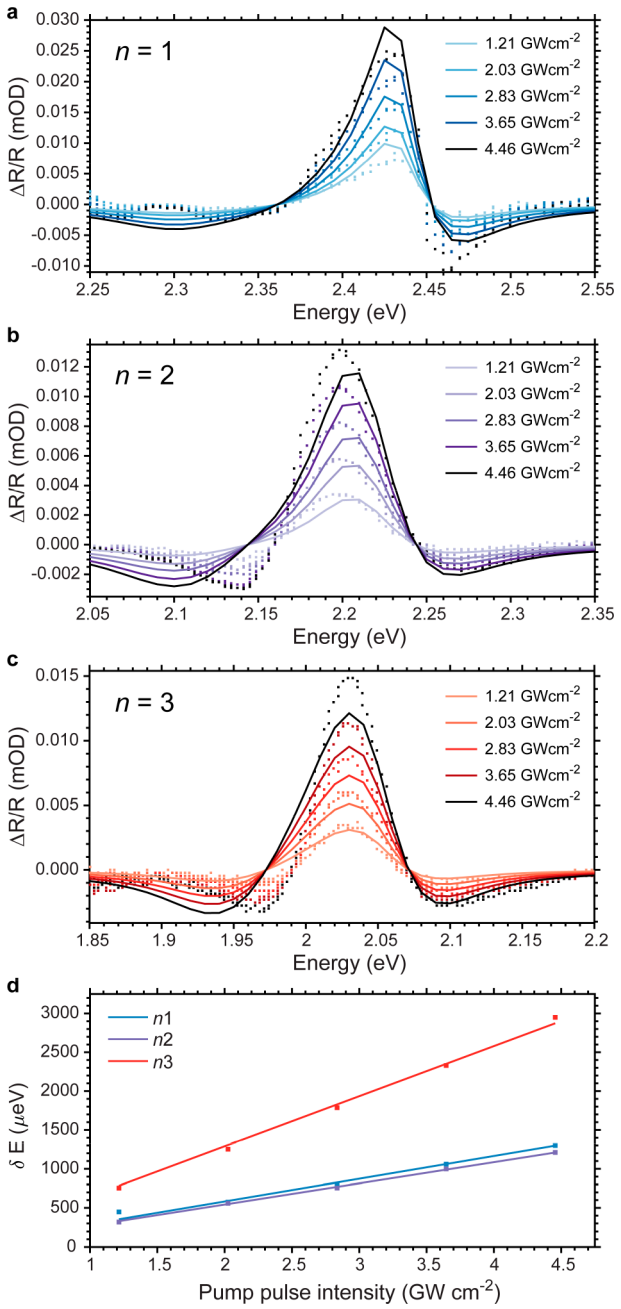

Figure 2. Fluence-dependent transient reflectance spectra for (a) n = 1, (b) n = 2, and (c) n = 3 single crystals. Spectra are taken at delay times corresponding to the maximum in the OSE signal (i.e., peak of the Gaussian fit of the temporal pump pulse profile). Experiments are performed with co- and cross-circularly polarized light at each pump fluence. The cross-polarized 2D transient reflectance maps are subtracted from the copolarized 2D maps, and spectral traces plotted here are taken from the residual map. Dotted lines correspond to raw transient reflectance data, and solid lines correspond to the fitted data. (d) Energy shift versus pump pulse intensity, showing the expected linear trend for all crystals.

Starting from the experimental crystallographic structures, we performed geometry optimization, relaxing the atomic positions and fixing the cell parameters to the experimental values (see Supporting Information for computational details). For the optimized geometries, a single-point calculation including spin−orbit coupling (SOC) was performed and the DOS of the n = 1−3 series were simulated, with results shown in Figure 3. The DOS shows a reduction of the band gap going from n = 1 to n = 3 due the simultaneous upshift of the valence

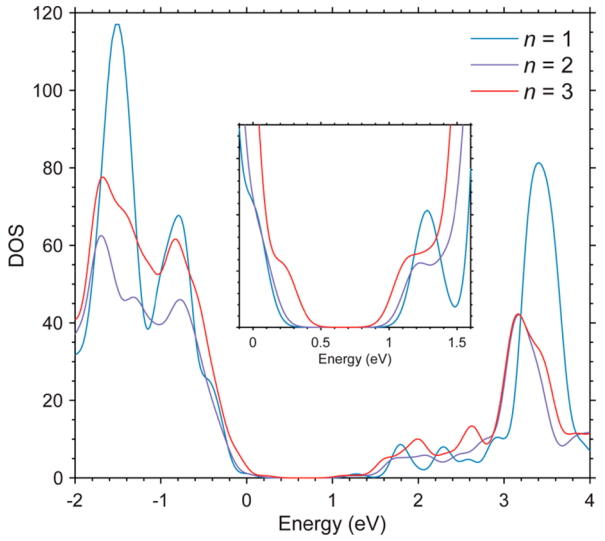

Figure 3. PBE-SOC DOS plot for n = 1−3. The inset shows the overview of the band gap region.

band (VB) and downshift of the conduction band (CB) (the DOS were aligned to the 5d orbitals of the Pb d atoms). Excitonic properties were addressed by solution of the Bethe−Salpter equation (BSE). BSE calculations require particularly dense sampling of the Brillouin zone for yielding converged excitonic properties such as the exciton binding energy and the corresponding transition dipole moment; it has been shown that exciton binding energies must be evaluated by extrapolating the results for increasing k-point density in the limit of continuum sampling.[53,54] We accomplished such an analysis only for the n = 2 system, for which a 6 × 6 × 1 k-mesh gives an exciton still localized in reciprocal space at the sole Γ point, giving a lower plane average transition dipole moment of 17.3 D. Extrapolating through a simple $1/N_{\text{k-point}}$ line yields an estimate of the converged transition dipole moment value for n = 2 of 16.5 D. For estimating the trends in the transition dipole moment on the same footing for all layered structures, we chose a smaller 2 × 2 × 2 k-point sampling because in this case all excitons are centered at the Γ point. We averaged the modulo of the transition dipoles over symmetrically equivalent excitations, finding values of 19.2, 18.9, and 22.7 D for the n = 1, 2, and 3 series, in agreement with the experimental trend (see Table 2). The calculated transition dipole moments of n = 1 and n = 3 scaled by the same factor as for n = 2 from coarse to converged k-mesh are equal to 16.8 and 19.8 D, respectively (see also Table 2).

In inorganic QW systems, a decreasing well thickness yields a higher exciton binding energy, owing to decreased electron−hole separation, and therefore higher oscillator strengths (proportional to the transition dipole moment).[55,56] As the QW is made sufficiently thin, the exciton binding energy reaches a maximum before it begins to decrease, as the exciton wave function starts to penetrate into the surrounding layers (e.g., for GaAs QWs with $Ga_{1-x}Al_xAs$ surrounding layers),[57] resulting in a nonmonotonic trend of QW width versus exciton binding energy and oscillator strength. Such a trend has also been observed for ZnCdSe/ZnSe QW heterostructures.[58] However, the PQWs studied herein are distinct from these

https://dx.doi.org/10.1021/acs.jpclett.9b03349
J. Phys. Chem. Lett. 2020, 11, 716−723

Table 2. Transition Dipole Moments Calculated for the First Four Excitations of n = 1, 2, and 3 Perovskites and BSE Excitation Energy (eV)[a]

crystal	Exc.	En.	x	y	z	x_{av}	y_{av}
n = 1	1	0.61	23.8	29.3	0.2	19.1	19.2
	2	0.61	18.3	16.5	0.0		
	3	0.61	18.4	16.8	0.1		
	4	0.61	14.8	7.6	0.0		
n = 2	1	0.70	26.0	22.5	0.5	18.9	18.9
	2	0.70	23.3	25.1	0.6		
	3	0.77	11.6	8.5	0.4		
	4	0.77	8.5	14.7	0.3		
n = 3	1	0.56	32.9	11.9	0.2	22.8	22.6
	2	0.58	18.0	33.3	0.3		
	3	0.59	25.1	16.9	0.2		
	4	0.59	5.9	22.4	0.3		

[a]Absolute contributions along the x, y, and z directions and the averages x_{av} and y_{av} along the x and y Cartesian directions corresponding to the in-plane perovskite directions are reported in Debye (D). A k-point mesh of 2 × 2 × 2 points has been used in the calculations. Extrapolated in-plane values of a converged k-point mesh are 16.8, 16.5, and 19.8 D for n = 1, 2, and 3, respectively

inorganic QW systems because they consist of exactly 1, 2, or 3 perovskite monolayers and therefore exist at or near the limit for 2D quantum confinement, rather than the multiple monolayers typically used in inorganic QWs. Furthermore, the PQW confining layers are composed of organic ligands rather than wider-band gap inorganic semiconductors, which may influence the extent to which the exciton wave function may penetrate into the surrounding layers. We find instead that in the n = 1, 2, and 3 PQWs, the trend of transition dipole moment versus QW width for the ground-state exciton is influenced by the degree of wave function delocalization.

Inspection of the wave function plots (Figure 4a–c) allows us to qualitatively understand the origin of the nonmonotonic variation of μ_{ge} with dimensionality. For all systems the electronic state corresponding to the lowest unoccupied molecular orbital (LUMO) is delocalized throughout the entire crystal. The n = 2 system shows a reduced μ_{ge} because of the delocalized wave function of the HOMO (and HOMO−1, irrespective of their energy separation) on the two PbI layers, while for n = 1 and n = 3 the HOMO is localized on a single PbI layer (which is obvious for n = 1, because there is only 1 PbI layer), with delocalized orbitals for n = 3 lying at lower energy. Because the transition dipole approximately scales as the overlap between starting (mainly HOMO) and arriving (mainly LUMO) orbitals involved in the excitation, a more localized starting orbital should give rise to stronger transitions. The n = 2 PQW must show a delocalized HOMO by construction because there is no preferential plane to localize the electron density, while such a plane exists for n = 1 and 3, giving rise to the odd–even alternation of transition dipole moments. We thus propose a different physical origin for the nonmonotonic trend of QW thickness versus oscillator strength in n = 1, 2, and 3 PQWs compared to inorganic QWs.

In sum, ultrafast transient reflectance spectroscopy and ellipsometry were performed on dimensionally pure single crystals of n = 1, 2, and 3 iodide-based PQWs. Through the optical Stark effect, we were able to extract values of the transition dipole moment for the PQW crystals. The experimentally measured values were found to be 11.1, 9.6, and 13.0 D for n = 1, 2, and 3, respectively. Our experimental results were corroborated by SOC-DFT and MBPT calculations, which supported a nonmonotonic trend of transition dipole magnitude versus PQW dimensionality. We attribute this to the n = 2 crystal structure exhibiting a more delocalized HOMO compared to n = 1 and n = 3, resulting in reduced overlap between the frontier orbitals involved in the band edge transition. The odd–even symmetry dependence of the transition dipole moment may prove to be important for dipole-mediated carrier-transfer processes and light emission in optoelectronic devices based on these materials.

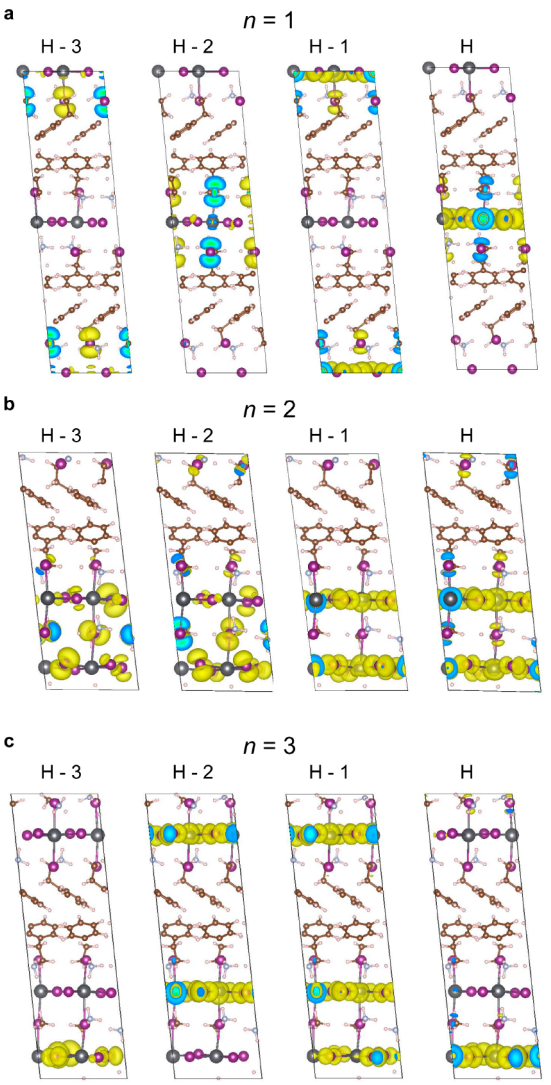

Figure 4. Wave function plots of the n = 1, 2, and 3 series at the PBE-SOC level of theory. Wave functions displayed are (from left to right): HOMO−3, HOMO−2, HOMO−1, and HOMO.

■ ASSOCIATED CONTENT

Supporting Information

The Supporting Information is available free of charge at https://pubs.acs.org/doi/10.1021/acs.jpclett.9b03349.

Materials and Methods and supplementary Figures S1–S3 (PDF)

https://dx.doi.org/10.1021/acs.jpclett.9b03349
J. Phys. Chem. Lett. 2020, 11, 716–723

AUTHOR INFORMATION

Corresponding Authors

Paolo Umari − *Università di Padova, Padova, Italy, and Consiglio Nazionale delle Ricerche, Trieste, Italy*; Email: paolo.umari@unipd.it

Osman M. Bakr − *King Abdullah University of Science and Technology, Thuwal, Kingdom of Saudi Arabia*; orcid.org/0000-0002-3428-1002; Email: osman.bakr@kaust.edu.sa

Edward H. Sargent − *University of Toronto, Toronto, Canada*; orcid.org/0000-0003-0396-6495; Email: ted.sargent@utoronto.ca

Other Authors

Andrew H. Proppe − *University of Toronto, Toronto, Canada*; orcid.org/0000-0003-3860-9949

Grant W. Walters − *University of Toronto, Toronto, Canada*; orcid.org/0000-0002-9005-2335

Abdullah Y. Alsalloum − *King Abdullah University of Science and Technology, Thuwal, Kingdom of Saudi Arabia*; orcid.org/0000-0001-8988-1307

Ayan A. Zhumekenov − *King Abdullah University of Science and Technology, Thuwal, Kingdom of Saudi Arabia*; orcid.org/0000-0002-3216-5315

Edoardo Mosconi − *Istituto CNR di Scienze e Tecnologie Chimiche "Giulio Natta" (CNR-SCITEC), Perugia, Italy*

Shana O. Kelley − *University of Toronto, Toronto, Canada*; orcid.org/0000-0003-3360-5359

Filippo De Angelis − *Istituto CNR di Scienze e Tecnologie Chimiche "Giulio Natta" (CNR-SCITEC), Perugia, Italy, and University of Perugia, Perugia, Italy*; orcid.org/0000-0003-3833-1975

Lyudmyla Adamska − *Università di Padova, Padova, Italy*; orcid.org/0000-0002-8098-6249

Complete contact information is available at: https://pubs.acs.org/10.1021/acs.jpclett.9b03349

Author Contributions

◆A.H.P. and G.W.W. contributed equally to this work.

Notes

The authors declare no competing financial interest.

ACKNOWLEDGMENTS

This publication is based on work supported by the United States Department of the Navy, Office of Naval Research (Grant Award No.: N00014-17-1-2524). A. H. P. and G. W. W. acknowledge support from the Natural Sciences and Engineering Research Council of Canada (NSERC). E.M. and F.D.A acknowledge European Union's Horizon 2020 research and innovation programme under Grant Agreement No. 764047 of the ESPRESSO project. The Ministero dell'Istruzione dell'Università e della Ricerca (MIUR) and Università degli Studi di Perugia are acknowledged for financial support through the program "Dipartimenti di Eccellenza 2018-2022" (Grant AMIS). L.A. and P.U. acknowledge PRACE (Project ID 20171633963) for awarding access to Marconi at CINECA, Italy.

REFERENCES

(1) Cho, K. T.; Paek, S.; Grancini, G.; Roldán-Carmona, C.; Gao, P.; Lee, Y.; Nazeeruddin, M. K. Highly Efficient Perovskite Solar Cells with a Compositionally Engineered Perovskite/Hole Transporting Material Interface. *Energy Environ. Sci.* **2017**, *10*, 621−627.

(2) Jeon, N. J.; Na, H.; Jung, E. H.; Yang, T.-Y.; Lee, Y. G.; Kim, G.; Shin, H.-W.; Il Seok, S.; Lee, J.; Seo, J. A Fluorene-Terminated Hole-Transporting Material for Highly Efficient and Stable Perovskite Solar Cells. *Nat. Energy* **2018**, *3*, 682−689.

(3) Jeon, N. J.; Noh, J. H.; Yang, W. S.; Kim, Y. C.; Ryu, S.; Seo, J.; Seok, S. I. Compositional Engineering of Perovskite Materials for High-Performance Solar Cells. *Nature* **2015**, *517*, 476−480.

(4) Byun, J.; Cho, H.; Wolf, C.; Jang, M.; Sadhanala, A.; Friend, R. H.; Yang, H.; Lee, T.-W. Efficient Visible Quasi-2D Perovskite Light-Emitting Diodes. *Adv. Mater.* **2016**, *28*, 7515−7520.

(5) Yuan, M.; Quan, L. N.; Comin, R.; Walters, G.; Sabatini, R.; Voznyy, O.; Hoogland, S.; Zhao, Y.; Beauregard, E. M.; Kanjanaboos, P.; et al. Perovskite Energy Funnels for Efficient Light-Emitting Diodes. *Nat. Nanotechnol.* **2016**, *11*, 872−877.

(6) Xiao, Z.; Kerner, R. A.; Zhao, L.; Tran, N. L.; Lee, K. M.; Koh, T.-W.; Scholes, G. D.; Rand, B. P. Efficient Perovskite Light-Emitting Diodes Featuring Nanometre-Sized Crystallites. *Nat. Photonics* **2017**, *11*, 108−115.

(7) Wang, N.; Cheng, L.; Ge, R.; Zhang, S.; Miao, Y.; Zou, W.; Yi, C.; Sun, Y.; Cao, Y.; Yang, R.; et al. Perovskite Light-Emitting Diodes Based on Solution-Processed Self-Organized Multiple Quantum Wells. *Nat. Photonics* **2016**, *10*, 699−704.

(8) Hu, H.; Salim, T.; Chen, B.; Lam, Y. M. Molecularly Engineered Organic-Inorganic Hybrid Perovskite with Multiple Quantum Well Structure for Multicolored Light-Emitting Diodes. *Sci. Rep.* **2016**, *6*, 33546.

(9) Zhu, H.; Fu, Y.; Meng, F.; Wu, X.; Gong, Z.; Ding, Q.; Gustafsson, M. V.; Trinh, M. T.; Jin, S.; Zhu, X.-Y. Lead Halide Perovskite Nanowire Lasers with Low Lasing Thresholds and High Quality Factors. *Nat. Mater.* **2015**, *14*, 636−642.

(10) Cao, D. H.; Stoumpos, C. C.; Farha, O. K.; Hupp, J. T.; Kanatzidis, M. G. 2D Homologous Perovskites as Light-Absorbing Materials for Solar Cell Applications. *J. Am. Chem. Soc.* **2015**, *137*, 7843−7850.

(11) Soe, C. M. M.; Stoumpos, C. C.; Kepenekian, M.; Traoré, B.; Tsai, H.; Nie, W.; Wang, B.; Katan, C.; Seshadri, R.; Mohite, A. D.; et al. New Type of 2D Perovskites with Alternating Cations in the Interlayer Space, $(C(NH_2)_3)(CH_3NH_3)_nPb_nI_{3n+1}$: Structure, Properties, and Photovoltaic Performance. *J. Am. Chem. Soc.* **2017**, *139*, 16297−16309.

(12) Quan, L. N.; Yuan, M.; Comin, R.; Voznyy, O.; Beauregard, E. M.; Hoogland, S.; Buin, A.; Kirmani, A. R.; Zhao, K.; Amassian, A.; et al. Ligand-Stabilized Reduced-Dimensionality Perovskites. *J. Am. Chem. Soc.* **2016**, *138*, 2649−2655.

(13) Maity, P.; Yin, J.; Cheng, B.; He, J.-H.; Bakr, O. M.; Mohammed, O. F. Layer-Dependent Coherent Acoustic Phonons in Two-Dimensional Ruddlesden−Popper Perovskite Crystals. *J. Phys. Chem. Lett.* **2019**, *10*, 5259−5264.

(14) Yin, J.; Maity, P.; Xu, L.; El-Zohry, A. M.; Li, H.; Bakr, O. M.; Brédas, J.-L.; Mohammed, O. F. Layer-Dependent Rashba Band Splitting in 2D Hybrid Perovskites. *Chem. Mater.* **2018**, *30*, 8538−8545.

(15) Ishihara, T.; Takahashi, J.; Goto, T. Exciton State in Two-Dimensional Perovskite Semiconductor (C10H21NH3)2PbI4. *Solid State Commun.* **1989**, *69*, 933−936.

(16) Ishihara, T.; Takahashi, J.; Goto, T. Optical Properties Due to Electronic Transitions in Two-Dimensional Semiconductors (CnH2n+1NH3)2PbI4. *Phys. Rev. B: Condens. Matter Mater. Phys.* **1990**, *42*, 11099−11107.

(17) Hong, X.; Ishihara, T.; Nurmikko, A. V. Dielectric Confinement Effect on Excitons in PbI4-Based Layered Semiconductors. *Phys. Rev. B: Condens. Matter Mater. Phys.* **1992**, *45*, 6961−6964.

(18) Hanamura, E.; Nagaosa, N.; Kumagai, M.; Takagahara, T. Quantum Wells with Enhanced Exciton Effects and Optical Non-Linearity. *Mater. Sci. Eng., B* **1988**, *1*, 255−258.
(19) Kato, Y.; Ichii, D.; Ohashi, K.; Kunugita, H.; Ema, K.; Tanaka, K.; Takahashi, T.; Kondo, T. Extremely Large Binding Energy of Biexcitons in an Organic−Inorganic Quantum-Well Material (C4H9NH3)2PbBr4. *Solid State Commun.* **2003**, *128*, 15−18.
(20) Blancon, J.-C.; Stier, A. V.; Tsai, H.; Nie, W.; Stoumpos, C. C.; Traoré, B.; Pedesseau, L.; Kepenekian, M.; Katsutani, F.; Noe, G. T.; et al. Scaling Law for Excitons in 2D Perovskite Quantum Wells. *Nat. Commun.* **2018**, *9*, 2254.
(21) Feldmann, J.; Peter, G.; Göbel, E. O.; Dawson, P.; Moore, K.; Foxon, C.; Elliott, R. J. Linewidth Dependence of Radiative Exciton Lifetimes in Quantum Wells. *Phys. Rev. Lett.* **1987**, *59*, 2337−2340.
(22) Wei, M.; Arquer, F. P. G. de; Walters, G.; Yang, Z.; Quan, L. N.; Kim, Y.; Sabatini, R.; Quintero-Bermudez, R.; Gao, L.; Fan, J. Z.; et al. Ultrafast Narrowband Exciton Routing within Layered Perovskite Nanoplatelets Enables Low-Loss Luminescent Solar Concentrators. *Nat. Energy* **2019**, *4*, 197.
(23) Liu, J.; Leng, J.; Wu, K.; Zhang, J.; Jin, S. Observation of Internal Photoinduced Electron and Hole Separation in Hybrid Two-Dimensional Perovskite Films. *J. Am. Chem. Soc.* **2017**, *139*, 1432−1435.
(24) Shang, Q.; Wang, Y.; Zhong, Y.; Mi, Y.; Qin, L.; Zhao, Y.; Qiu, X.; Liu, X.; Zhang, Q. Unveiling Structurally Engineered Carrier Dynamics in Hybrid Quasi-Two-Dimensional Perovskite Thin Films toward Controllable Emission. *J. Phys. Chem. Lett.* **2017**, *8*, 4431−4438.
(25) Proppe, A. H.; Elkins, M. H.; Voznyy, O.; Pensack, R. D.; Zapata, F.; Besteiro, L. V.; Quan, L. N.; Quintero-Bermudez, R.; Todorovic, P.; Kelley, S. O.; et al. Spectrally Resolved Ultrafast Exciton Transfer in Mixed Perovskite Quantum Wells. *J. Phys. Chem. Lett.* **2019**, *10*, 419−426.
(26) Scholes, G. D. Long-Range Resonance Energy Transfer in Molecular Systems. *Annu. Rev. Phys. Chem.* **2003**, *54*, 57−87.
(27) Krueger, B. P.; Scholes, G. D.; Fleming, G. R. Calculation of Couplings and Energy-Transfer Pathways between the Pigments of LH2 by the Ab Initio Transition Density Cube Method. *J. Phys. Chem. B* **1998**, *102*, 5378−5386.
(28) Förster, T. *Delocalized Excitation and Excitation Transfer*; Florida State University, 1965.
(29) Medintz, I. L.; Hildebrandt, N. *FRET - Förster Resonance Energy Transfer: From Theory to Applications*; John Wiley & Sons, 2013.
(30) Lyo, S. K. Energy Transfer of Excitons between Quantum Wells Separated by a Wide Barrier. *Phys. Rev. B: Condens. Matter Mater. Phys.* **2000**, *62*, 13641−13656.
(31) Brumberg, A.; Harvey, S. M.; Philbin, J. P.; Diroll, B. T.; Lee, B.; Crooker, S. A.; Wasielewski, M. R.; Rabani, E.; Schaller, R. D. Determination of the In-Plane Exciton Radius in 2D CdSe Nanoplatelets via Magneto-Optical Spectroscopy. *ACS Nano* **2019**, *13*, 8589−8596.
(32) Prins, F.; Goodman, A. J.; Tisdale, W. A. Reduced Dielectric Screening and Enhanced Energy Transfer in Single- and Few-Layer MoS2. *Nano Lett.* **2014**, *14*, 6087−6091.
(33) Schuller, J. A.; Karaveli, S.; Schiros, T.; He, K.; Yang, S.; Kymissis, I.; Shan, J.; Zia, R. Orientation of Luminescent Excitons in Layered Nanomaterials. *Nat. Nanotechnol.* **2013**, *8*, 271−276.
(34) Gao, Y.; Weidman, M. C.; Tisdale, W. A. CdSe Nanoplatelet Films with Controlled Orientation of Their Transition Dipole Moment. *Nano Lett.* **2017**, *17*, 3837−3843.
(35) Rowland, C. E.; Fedin, I.; Zhang, H.; Gray, S. K.; Govorov, A. O.; Talapin, D. V.; Schaller, R. D. Picosecond Energy Transfer and Multiexciton Transfer Outpaces Auger Recombination in Binary CdSe Nanoplatelet Solids. *Nat. Mater.* **2015**, *14*, 484−489.
(36) Hilborn, R. C. Einstein Coefficients, Cross Sections, f Values, Dipole Moments, and All That. *Am. J. Phys.* **1982**, *50*, 982−986.
(37) Li, M.; Gao, Q.; Liu, P.; Liao, Q.; Zhang, H.; Yao, J.; Hu, W.; Wu, Y.; Fu, H. Amplified Spontaneous Emission Based on 2D Ruddlesden−Popper Perovskites. *Adv. Funct. Mater.* **2018**, *28*, 1707006.
(38) Sie, E. J.; McIver, J. W.; Lee, Y.-H.; Fu, L.; Kong, J.; Gedik, N. Valley-Selective Optical Stark Effect in Monolayer WS_2. *Nat. Mater.* **2015**, *14*, 290−294.
(39) Autler, S. H.; Townes, C. H. Stark Effect in Rapidly Varying Fields. *Phys. Rev.* **1955**, *100*, 703−722.
(40) Shirley, J. H. Solution of the Schrodinger Equation with a Hamiltonian Periodic in Time. *Phys. Rev.* **1965**, *138*, B979−B987.
(41) Giovanni, D.; Chong, W. K.; Dewi, H. A.; Thirumal, K.; Neogi, I.; Ramesh, R.; Mhaisalkar, S.; Mathews, N.; Sum, T. C. Tunable Room-Temperature Spin-Selective Optical Stark Effect in Solution-Processed Layered Halide Perovskites. *Sci. Adv.* **2016**, *2*, No. e1600477.
(42) Yang, Y.; Yang, M.; Zhu, K.; Johnson, J. C.; Berry, J. J.; van de Lagemaat, J.; Beard, M. C. Large Polarization-Dependent Exciton Optical Stark Effect in Lead Iodide Perovskites. *Nat. Commun.* **2016**, *7*, 12613.
(43) Peng, W.; Yin, J.; Ho, K.-T.; Ouellette, O.; De Bastiani, M.; Murali, B.; El Tall, O.; Shen, C.; Miao, X.; Pan, J.; et al. Ultralow Self-Doping in Two-Dimensional Hybrid Perovskite Single Crystals. *Nano Lett.* **2017**, *17*, 4759−4767.
(44) Shi, D.; Adinolfi, V.; Comin, R.; Yuan, M.; Alarousu, E.; Buin, A.; Chen, Y.; Hoogland, S.; Rothenberger, A.; Katsiev, K.; et al. Low Trap-State Density and Long Carrier Diffusion in Organolead Trihalide Perovskite Single Crystals. *Science* **2015**, *347*, 519−522.
(45) Saidaminov, M. I.; Abdelhady, A. L.; Murali, B.; Alarousu, E.; Burlakov, V. M.; Peng, W.; Dursun, I.; Wang, L.; He, Y.; Maculan, G.; et al. High-Quality Bulk Hybrid Perovskite Single Crystals within Minutes by Inverse Temperature Crystallization. *Nat. Commun.* **2015**, *6*, 7586.
(46) Von Lehmen, A.; Chemla, D. S.; Zucker, J. E.; Heritage, J. P. Optical Stark Effect on Excitons in GaAs Quantum Wells. *Opt. Lett.* **1986**, *11*, 609−611.
(47) Tai, K.; Hegarty, J.; Tsang, W. T. Observation of Optical Stark Effect in InGaAs/InP Multiple Quantum Wells. *Appl. Phys. Lett.* **1987**, *51*, 152−154.
(48) Song, D.; Wang, F.; Dukovic, G.; Zheng, M.; Semke, E. D.; Brus, L. E.; Heinz, T. F. Measurement of the Optical Stark Effect in Semiconducting Carbon Nanotubes. *Appl. Phys. A: Mater. Sci. Process.* **2009**, *96*, 283−287.
(49) Peng, W.; Yin, J.; Ho, K.-T.; Ouellette, O.; De Bastiani, M.; Murali, B.; El Tall, O.; Shen, C.; Miao, X.; Pan, J.; et al. Ultralow Self-Doping in Two-Dimensional Hybrid Perovskite Single Crystals. *Nano Lett.* **2017**, *17*, 4759−4767.
(50) Quintero-Bermudez, R.; Gold-Parker, A.; Proppe, A. H.; Munir, R.; Yang, Z.; Kelley, S. O.; Amassian, A.; Toney, M. F.; Sargent, E. H. Compositional and Orientational Control in Metal Halide Perovskites of Reduced Dimensionality. *Nat. Mater.* **2018**, *17*, 900.
(51) Sie, E. J.; McIver, J. W.; Lee, Y.-H.; Fu, L.; Kong, J.; Gedik, N. Valley-Selective Optical Stark Effect in Monolayer WS 2. *Nat. Mater.* **2015**, *14*, 290−294.
(52) Giannozzi, P.; Baroni, S.; Bonini, N.; Calandra, M.; Car, R.; Cavazzoni, C.; Ceresoli, D.; Chiarotti, G. L.; Cococcioni, M.; Dabo, I.; et al. QUANTUM ESPRESSO: A Modular and Open-Source Software Project for Quantum Simulations of Materials. *J. Phys.: Condens. Matter* **2009**, *21*, 395502.
(53) Umari, P.; Mosconi, E.; De Angelis, F. Infrared Dielectric Screening Determines the Low Exciton Binding Energy of Metal-Halide Perovskites. *J. Phys. Chem. Lett.* **2018**, *9*, 620−627.
(54) Bokdam, M.; Sander, T.; Stroppa, A.; Picozzi, S.; Sarma, D. D.; Franchini, C.; Kresse, G. Role of Polar Phonons in the Photo Excited State of Metal Halide Perovskites. *Sci. Rep.* **2016**, *6*, 28618.
(55) Gurioli, M.; Martinez-Pastor, J.; Colocci, M.; Bosacchi, A.; Franchi, S.; Andreani, L. C. Well-Width and Aluminum-Concentration Dependence of the Exciton Binding Energies in GaAs/AlxGa1-XAs Quantum Wells. *Phys. Rev. B: Condens. Matter Mater. Phys.* **1993**, *47*, 15755−15762.

https://dx.doi.org/10.1021/acs.jpclett.9b03349
J. Phys. Chem. Lett. 2020, 11, 716−723

(56) Matsuura, M.; Kamizato, T. Oscillator Strength of Excitons in Quantum Wells. *Surf. Sci.* **1986**, *174*, 183−187.
(57) Greene, R. L.; Bajaj, K. K.; Phelps, D. E. Energy Levels of Wannier Excitons in GaAs−Ga1−xAlxAs Quantum-Well Structures. *Phys. Rev. B: Condens. Matter Mater. Phys.* **1984**, *29*, 1807−1812.
(58) Senger, R. T.; Bajaj, K. K. Binding Energies of Excitons in Polar Quantum Well Heterostructures. *Phys. Rev. B: Condens. Matter Mater. Phys.* **2003**, *68*, 205314.

https://dx.doi.org/10.1021/acs.jpclett.9b03349
J. Phys. Chem. Lett. 2020, 11, 716−723